Plant Physiology and Biochemistry 194 (2023) 361–373

Contents lists available at ScienceDirect

Plant Physiology and Biochemistry

journal homepage: www.elsevier.com/locate/plaphy

Hormetic activation of nano-sized rare earth element terbium on growth, PSII photochemistry, antioxidant status and phytohormone regulation in *Lemna minor*

Fatma Nur Alp [a], Busra Arikan [a], Ceyda Ozfidan-Konakci [b], Cagri Gulenturk [a], Evren Yildiztugay [a,*], Metin Turan [c], Halit Cavusoglu [d]

[a] Department of Biotechnology, Faculty of Science, Selcuk University, Selcuklu, 42130, Konya, Turkey
[b] Department of Molecular Biology and Genetics, Faculty of Science, Necmettin Erbakan University, Meram, 42090, Konya, Turkey
[c] Department of Agricultural Trade and Management, Faculty of Economy and Administrative Sciences, Yeditepe University, 34755, İstanbul, Turkey
[d] Department of Physics, Faculty of Science, Selcuk University, Selcuklu, 42130, Konya, Turkey

ARTICLE INFO

Keywords:
Antioxidant
Chlorophyll fluorescence
Hormetic effect
Lemna minor
Nano-size terbium

ABSTRACT

Soils contaminated with rare earth elements (REEs) can damage agriculture by causing physiological disorders in plants which are evaluated as the main connection of the human food chain. A biphasic dose response with excitatory responses to low concentrations and inhibitory/harmful responses to high concentrations has been defined as hormesis. However, not much is clear about the ecological effects and potential risks of REEs to plants. For this purpose, here we showed the impacts of different concentrations of nano terbium (Tb) applications (5-10-25-50-100-250-500 mg L^{-1}) on the accumulation of endogeneous certain ions and hormones, chlorophyll fluoresence, photochemical reaction capacity and antioxidant activity in duckweed (*Lemna minor*). Tb concentrations less than 100 mg L^{-1} increased the contents of nitrogen (N), phosphate (P), potassium (K^+), calcium (Ca^{2+}), magnesium (Mg^{2+}), manganese (Mn^{2+}) and iron (Fe^{2+}). Chlorophyll fluorescence (F_v/F_m and F_v/F_o) was suppressed under 250–500 mg L^{-1} Tb. In addition, Tb toxicity affected the trapped energy adversely by the active reaction center of photosystem II (PSII) and led to accumulation of inactive reaction centers, thus lowering the detected level of electron transport from photosystem II (PSII) to photosystem I (PSI). On the other hand, 5–100 mg L^{-1} Tb enhanced the activities of superoxide dismutase (SOD), catalase (CAT), peroxidase (POX), NADPH oxidase (NOX), ascorbate peroxidase (APX), glutathione reductase (GR), monodehydroascorbate reductase (MDHAR), dehydroascorbate reductase (DHAR) and glutathione *S*-transferase (GST). Tb (5–50 mg L^{-1}) supported the maintenance of cellular redox status by promoting antioxidant pathways involved in the ascorbate-glutathione (AsA-GSH) cycle. In addition to the antioxidant system, the contents of some hormones such as indole-3-acetic acid (IAA), gibberellic acid (GA), cytokinin (CK) and salicylic acid (SA) were also induced in the presence of 5–100 mg L^{-1} Tb. In addition, the levels of hydrogen peroxide (H_2O_2) and lipid peroxidation (TBARS) were controlled through ascorbate (AsA) regeneration and effective hormonal modulation in *L. minor*. However, this induction in the antioxidant system and phytohormone contents could not be resumed after applications higher than 250 mg L^{-1} Tb. TBARS and H_2O_2, which indicate the level of lipid peroxidation, increased. The results in this study showed that Tb at appropriate concentrations has great potential to confer tolerance of duckweed by supporting the antioxidant system, protecting the biochemical reactions of photosystems and improving hormonal regulation.

1. Introduction

Rare earth elements (REEs) represent Group IIIA elements consisting of lanthanides, scandium and yttrium. REEs are commonly used in new advanced technologies, including electronics, chemical engineering, renewable energy, medical applications and agricultural fertilizers

* Corresponding author.
E-mail addresses: fatmanur.alp@selcuk.edu.tr (F.N. Alp), busra.arikan@selcuk.edu.tr (B. Arikan), cozfidan@erbakan.edu.tr (C. Ozfidan-Konakci), 3816cagri@gmail.com (C. Gulenturk), eytugay@selcuk.edu.tr (E. Yildiztugay), metin.turan@yeditepe.edu.tr (M. Turan), hcavusoglu@selcuk.edu.tr (H. Cavusoglu).

https://doi.org/10.1016/j.plaphy.2022.11.031
Received 26 August 2022; Received in revised form 23 November 2022; Accepted 24 November 2022
Available online 28 November 2022

(Syrvatka et al., 2022). Terbium (Tb), from the lanthanide group, is used in various industries, so Tb is inevitably present in the environment. Therefore, Tb can come into direct contact with plants and accumulate in plant tissues (Loktyushkin et al., 2019).

Researches of the underlying mechanisms and biological outcomes of plant stress have grounded the core of modern plant science field. The biological consequences of stress can be tackled by exposing organisms to different doses of stress factors. Recently, such a dose-response study can ensure important information for plant stress mechanism, risk assessment and policy making (Agathokleous et al., 2019). Late reports have demonstrated that hormesis, a biphasic dose response with stimulus responses to low concentrations and inhibitory/harmful responses to high concentrations, eventuates widely (Agathokleous et al., 2019). In the studies carried out, the hormetic effects of changing amounts of REEs on growth and expressions of oxidative stress in aquaculture were evaluated. The alterations such as increased seed germination and biomass were detected at low REE doses, while higher REE exposures were associated with an augmented thiobarbituric acid reactive substances (TBARS) and hydrogen peroxide (H_2O_2) and a diminished chlorophyll content, soluble proteins and photosynthetic activity (Liu et al., 2012a). Several studies showed that REEs and their compounds at suitable concentrations may improve the stress endurance of plants by supporting cellular defense mechanisms, thereby alleviating the phytotoxicity of abiotic stress factors (Liu et al., 2013). Previous examples demonstrated the efficacy of REEs in improving photosynthesis in plants by detecting that lanthanum and cerium concentrations between 25 and 50 μM upregulated the chlorophyll fluorescence and photosynthetic activity of *Zea mays* and increased the Chl *a* amount and photosynthetic potential of *Glycine max*, rice and horseradish (Cao et al., 2017; Liu et al., 2012b; Wang et al., 2014). In addition, REEs applied at appropriate doses induce antioxidant metabolism in *Oryza sativa* and *Helianthus annuus* (Dridi et al., 2022; Liu et al., 2012b). However, exposure to high concentrations of REEs may result in increased accumulation of reactive oxygen species (ROS) that cause oxidative stress in plants. This oxidative stress can lead to an imbalanced plant metabolism, causing impairment of plant growth and photosynthesis (Zulfiqar and Ashraf, 2022). For instance, adverse impacts of increasing level of lanthanum applications reported, showing a significant reduction in the growth and antioxidant activity of *Triticum durum* (d'Aquino et al., 2009). In addition, the reported decreases in Chl *a* and, Chl *b* contents and net photosynthesis rate of *Oryza sativa* treated with different concentrations of lanthanum are due to the damage induced by that REE in the ultrastructure of the chloroplasts (Hu et al., 2016).

The synthesis method of nanoparticles (NPs) plays a crucial role in their application in biological systems. In pursuit of the synthesis of non-toxic, clean and environmentally friendly NPs, green technology appears to be the most promising method. NPs produced with green technology have many benefits such as larger surface area, more catalytic activity and provide better contact with biological process (Salem and Fouda, 2021). On the other hand, nano-size REEs have a high prerogative in agricultural applications because of their unique properties, including faster transport across membranes and high surface area. There are both positive and negative reports about the role of nano-scale rare earth elements under stress or non-stress conditions. Additionally, nano-size REEs have the capability to enhance development and growth of plants. Also, they trigger seed emergence by controlling availability of beneficial nutrients and stimulate the photosynthetic reactions (Ramos et al., 2016). To alleviate the effects of abiotic stresses, rare earth oxide NPs may act as a scavenger of free oxygen radicals and activate antioxidant systems. Ma et al. (2015) revealed a regression in the elongation of roots and shoots in cucumber exposed to nano-lanthanum. Besides that, the response of plants to terbium (Tb) stress is quite a complicated case that can lead to inhibited growth and physiological/biochemical disturbances (Rodziewicz et al., 2014). Human exposure to REEs occurs via ingestion of contaminated water and food, inhalation, and direct intake during medical administration (Gwenzi et al., 2018).

Lemnaceae family, which has a large amount of biomass, are the smallest and fastest growing angiosperms in the world. They have outstanding economic potential and can be used in many practical applications in biotechnology and ecology related researches. Also, their morphological and physiological properties enable to valued bioassays under limited conditions in a short time. Therefore, they represent model laboratory organisms. *Lemna* species are appropriate bioindicators for *in vivo* and *in vitro* ecotoxicological tests (Basiglini et al., 2018). Earlier, the effects of REEs on antioxidant activity and growth in an aquatic species *Lemna minor* (duckweed) thoroughly studied for biomonitoring and bioremediation of pollutants in freshwater, were investigated (Zicari et al., 2018). However, in order to protect the plants from oxidative stress, the antioxidant defense system, which includes enzymatic compounds such as superoxide dismutase (SOD), catalase (CAT), peroxidase (POX) and non-enzymatic components of glutathione, carotenoids and ascorbate, is immediately activated and participates in reactive oxygen species (ROS) detoxification (Kovaříková et al., 2019). Simultaneously with this system, plant phytohormones such as abscisic acid (ABA), indole acetic acid (IAA) and salicylic acid (SA) have important functions that control and regulate plant metabolism and development through various biochemical and physiological pathways. Depending on environmental stimuli, these hormones can act in places close to or far from where they are. Therefore, hormones are of vital importance in avoiding abiotic stress (Rhaman et al., 2020).

Terbium oxide nanoparticles are suitable as a representative element to examine the effects of REEs on plants (Ion et al., 2021). However, none of the studies provided information about the beneficial/harmful effects of nano-size terbium on the capacity of photosystems and antioxidant activity in plants. Therefore, the main objective of this study was to evaluate the hormetic responses caused by exposure to different terbium oxide nanoparticle concentrations in *Lemna minor* plants: (i) analysis of chlorophyll *a* fluorescence transient; (ii) examining the degree of cellular damage by determining the levels of H_2O_2 and TBARS; (iii) evaluation of antioxidant enzyme efficiency and phytohormone contents; and (iv) evaluation of sensitivity of potential retention of REEs in *L. minor* plants.

2. Material and methods

2.1. Synthesis procedures and characterization of nano-size Tb

Terbium (III) acetate hydrate, $Tb(CH_3CO_2)_3xH_2O$, was purchased from Sigma–Aldrich with 98% purity. The analytical reagents HNO_3, NaOH, and absolute ethanol were all employed without further purification. Nanocrystalline Tb_4O_7 was synthesized using the thermal decomposition of terbium acetate precursor, which was prepared by the precipitation method using NaOH as a precipitant according to the literature (Soliman and Abu-Zied, 2009). It was calcined at 800 °C, in air atmosphere, for 3 h. The morphologies of the samples were characterized by scanning electron microscopy (SEM, Zeiss Jeol Evo LS 10, Oberkochen, Germany) with X-ray energy dispersive spectrometry (EDX). Fourier transform infrared spectrum (FTIR) was recorded on a Vertex 70 Bruker FTIR spectrometer (Bruker, Germany). All spectra were captured in the 400 and 4000 cm^{-1} spectral region at a scan rate of 180 scans and a spectral resolution of 4 cm^{-1}. The transmittance mode made use of the FTIR spectrum.

2.2. Experimental design and treatments

Duckweed (*Lemna minor* L.) cultures were grown in hydroponic Hoagland solution under controlled conditions (16/8 h light/dark regime at 24 °C, 70% relative humidity and 350 μmol m^{-2} s^{-1} photosynthetic photon flux density) and the solutions were refreshed every three days. For nano-size terbium applications, Tb-5, Tb-10, Tb-25, Tb-50, Tb-100, Tb-250 and Tb-500 (5-10-25-50-100-250-500 mg L^{-1} nano-size Tb, respectively) were chosen based on the studies reported by

Wang et al. (2009) and Liu et al. (2022). Plants were harvested after a one-week treatment period and rinsed with deionized water.

2.3. Determination of relative growth rate

The relative growth rate (RGR) values were calculated according to the formula suggested by Hunt et al. (2002);

$$RGR = [\ln (DW_2) - \ln (DW_1)] / (t_2 - t_1),$$

where DW_1 = dry weight (g) at t_1, DW_2 = dry weight (g) at t_2, t_1 is initial harvest, and t_2 is final harvest.

2.4. Endogenous content/accumulation of some ions and nano-size Tb

The ion content was measured by Varian Vista-MPX simultaneous inductively coupled plasma optical emission spectrometer (ICP-OES) (Nyomora et al., 1997).

2.5. Photosystem II efficiency and OJIP analysis

The changes in the photochemistry of PSII were detected by Handy PEA (Plant Efficiency Analyser, Hansatech Instruments Ltd.). Supplementary Table S1 includes the descriptions for the calculated parameters. The average parameter values of treatment groups in *L. minor* were illustrated in the radar plots.

2.6. Determination of H_2O_2 and TBARS contents

H_2O_2 contents, which is one of the reactive oxygen species, were calculated according to Cheeseman (2006)'s method. The H_2O_2 content of the leaves was measured using the eFOX reagent (250 μM ferroammonium sulfate, 100 μM xylenol orange, 100 μM sorbitol and 1% ethanol (v/v)). Cold acetone containing 25 mM H_2SO_4 was used for extraction. Samples were centrifuged at 3,000×*g* for 5 min at 4 °C and 950 μL of eFOX reagent was used for 50 μL of supernatant. The reaction mixture was incubated for 30 min at room temperature. Then, absorbance measurements were performed at 550 and 800 nm. The H_2O_2 concentrations in the samples were calculated according to the standard slope graph prepared according to the known H_2O_2 amounts.

Lipid peroxidation (TBARS) changes, which best indicate the severity of damage under stress, were determined by measuring malondialdehyde (MDA) equivalents content. The TBARS content was measured with minor modifications to the method of Rao and Sresty (2000). For this, 0.5 g of the leaf sample, which was shocked, was homogenized with trichloroacetic acid (TCA). After centrifugation at 10,000g × 5 min, the reaction mixture containing thiobarbituric acid (TBA) and TCA was pipetted into the supernatant transferred to the tubes and heated at 95 °C for 45 min. After cooling, the mixture was centrifuged at 10,000g × 15 min. Then, the absorbance values of the supernatant at 532 and 600 nm were read. The TBARS concentration was calculated using the extinction coefficient $\epsilon = 155\ mM^{-1}\ cm^{-1}$ and expressed as nmol g^{-1} fresh weight.

2.7. Determination of enzymatic/non-enzymatic antioxidants

For protein and enzyme extractions, 0.5 g of each leaf sample was homogenized in 50 mM Tris-HCl (pH 7.8) containing 0.1 mM ethylenediaminetetraacetic acid (EDTA), 0.2% Triton X-100, 1 mM phenylmethylsulfonyl fluoride and 2 mM dithiothreitol (DTT). The total soluble protein content of the enzyme extracts was determined (Bradford, 1976). Superoxide dismutase (SOD) isozyme/enzyme activity was defined (Beauchamp and Fridovich, 1971; Laemmli, 1970). The activity of catalase (CAT) isozyme/enzyme was determined using the procedure suggested by Woodbury et al. (1971) and Bergmeyer (1970). The isozymes/enzyme capacity of peroxidase (POX) was measured according to the method suggested by Seevers et al. (1971) and Herzog and Fahimi (1973). The enzyme/isozyme activities of glutathione *S*-transferase (GST) and glutathione peroxidase (GPX) were determined (Hossain et al., 2006; Ricci et al., 1984). The isoforms and total NADPH oxidase (NOX) activity were calculated (Jiang and Zhang, 2002; Sagi and Fluhr, 2001).

Ascorbate peroxidase (APX) and glutathione reductase (GR) were spectrophotometrically and electrophoretically carried out (Mittler and Zilinskas, 1993; Nakano and Asada, 1981). The contents of ascorbate (AsA) and oxidized ascorbate (DHA) were estimated (Dutilleul et al., 2003). The Dutilleul et al. (2003) method was applied for the activity of monodehydroascorbate reductase (MDHAR) and dehydroascorbate reductase (DHAR) enzymes. Glutathione (GSH) was assayed according to Paradiso et al. (2008), utilizing aliquots of supernatant neutralized with 0.5 M K–P buffer. Based on enzymatic recycling, glutathione is oxidized by DTNB and reduced by NADPH in the presence of GR, and glutathione content is evaluated by the rate of absorption changes at 412 nm. Oxidized glutathione (GSSG) was determined after the removal of GSH by 2-vinylpyridine derivatization. Standard curves with known concentrations of GSH and GSSG were used for the quantification. GSH redox status was obtained (Shi et al., 2013).

The Gel Doc XR + System was used to photograph stained gels and subsequently evaluated using Image Lab software v4.0.1 (Bio-Rad, California, USA). Enzyme standards were used in gels for normalization.

2.8. GC-MS analysis and hormone contents

Extraction and purification processes were executed as described by Kuraishi et al. (1991) and Battal and Tileklioglu (2001). Methanol 80% at −40 °C was added to fresh leaf samples. After the material was homogenized for 10 min with Ultra Turrax, it was incubated for 24 h in the dark. The samples were filtered through Whatman No. 1 filter paper and the supernatants were filtered again through a 0.45-μm pore filter (Cutting, 1991). Supernatants were dried at 35 °C using an evaporator pump. Dried supernatants were dissolved in 0.1 M KH_2PO_4 (pH 8.0). Extracts were centrifuged at 5000 rpm for 1 h at 4 °C to separate fatty acids (Palni et al., 1983). Polyvinylpyrrolidone (PVPP), 1 g, was added to the supernatant to separate phenolic and colored materials (Hernandez-Miñana, 1991; Qamaruddin, 1991). The supernatant was then filtered through Whatman No. 1 paper to remove the PVPP (Cheikh and Jones, 1994). For further specific separation, a Sep-Pak C-18 (Waters) cartridge was used. Hormones absorbed by the cartridge were transferred to vials using 80% methanol. The hormones were analyzed by high performance liquid chromatography (HPLC) using a Zorbax Eclipse-AAA C-18 column (Agilent 1200 HPLC) and by absorbance at 265 nm in a UV detector. Flow speed was set to 1.2 mL min^{-1} at a column temperature of 25 °C. Hormone levels were determined using 13% acetonitrile (pH 4.98) as the mobile phase.

2.9. Statical analysis

The information on statical analysis was given in Supplementary Table S1.

3. Results

3.1. Nano-size Tb characterization

Fig. 1A–C demonstrated the SEM images of the nanocrystalline Tb, control plant sample and the 500 mg L^{-1} nano size Tb-applied plants, respectively. Fig. 1A depicts the surface morphology of the nanocrystalline Tb as observed by SEM. The surface of Tb nanocrystalline particles consists of crystals randomly oriented, varying in dimensions, and having sharp edges. Additionally, smaller, irregular crystals with some cracks can be seen. As a result of the incorporation of nanocrystalline Tb into the plant environment, a dramatic morphological

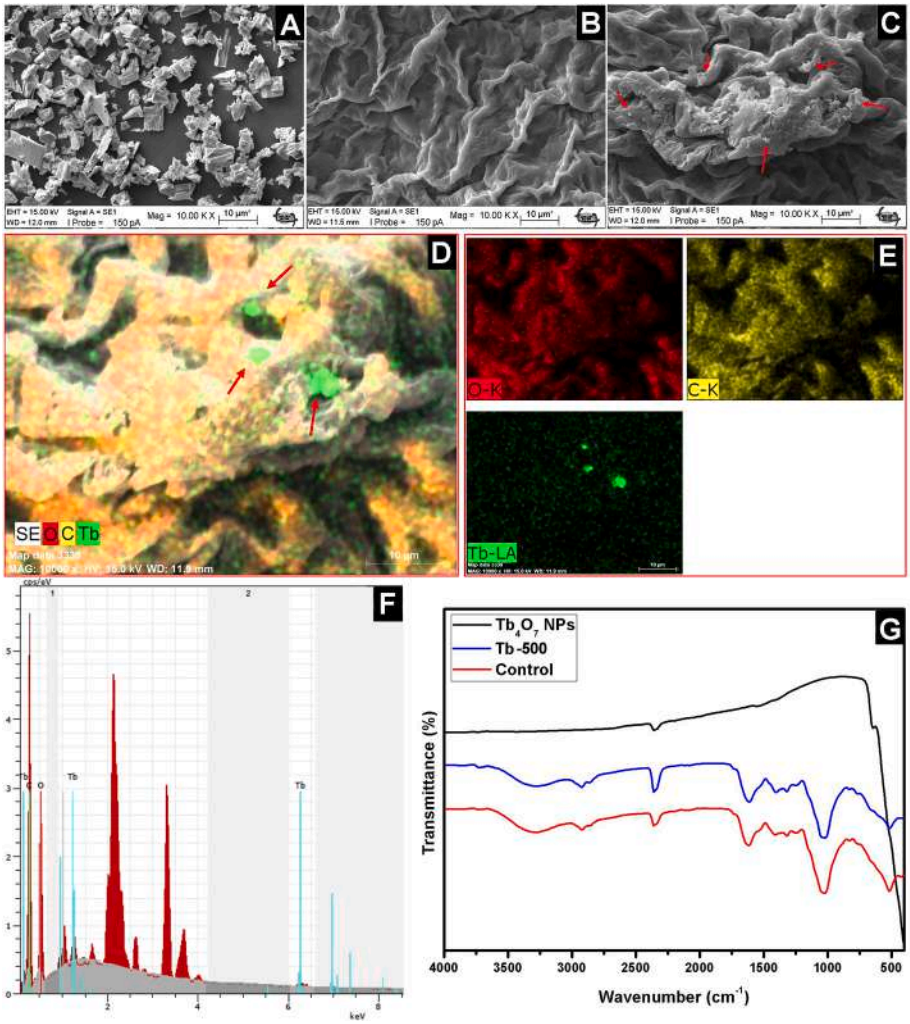

Fig. 1. SEM images of nano-size Tb (**A**), control plant sample (**B**), and the plants exposed to 500 mg L^{-1} nano-size Tb (**C**). SEM–EDX elemental mapping images of nano-size Tb incorporated plant exposed to 500 mg L^{-1} nano-size Tb (**D, E**), SEM–EDX spectrum of the nano-size Tb incorporated plant exposed to 500 mg L^{-1} nano-size Tb (**F**). These elemental mapping images are from the same tissue in each plant. FT-IR analysis of prepared nano-size Tb, control plant sample, plant exposed to 500 mg L^{-1} nano-size Tb (**G**).

change has occurred, as seen in Fig. 1B–C compared to the images of the control plant sample. Besides, SEM mapping and EDX spectra have been used to analyze the distribution of all elements, their compositions, and their existence in addition to dopant element. EDX is a valid method for demonstrating the existence of elements and their configuration in the samples, while mapping shows the uniform distribution of each element in the prepared samples. Hence, the SEM mapping and EDX spectrum were carried out and displayed in Fig. 1D–E, respectively. SEM mapping images displayed in Fig. 1D–E for the plants exposed to 500 mg L^{-1} nano-size Tb indicated that C, O and Tb are well diffused throughout the samples. As seen in Fig. 1F, O map is in red, C in yellow and Tb in green colour and their combination shown in Fig. 1D confirms the homogeneity of the prepared sample. In order to identify the functional groups produced by the integration of nano-size Tb into the plant samples, a comparative investigation utilizing FT-IR spectroscopy was also carried out. Fig. 1G depicted the FT-IR spectra of the pristine nano-size Tb, pure plant sample and interpretation of the adhesion of the produced nano-size Tb to plant samples. As shown in Fig. 1G, nano-size Tb exhibit an absorption band at 2357 cm^{-1}, this is assigned to the ν(N–C═O) stretching vibration. In the meantime, the ν(O–H) stretching vibration cannot be observed because of the thermal decomposition synthesis procedure of nano-size Tb. Different vibrational peaks of altered intensities were detected and were assigned to various functional groups for the control plant samples and nano-size Tb incorporated plants treated with 500 mg L^{-1} nano-size Tb (TB-500) in Fig. 1G. The vibrational peaks at 3277 cm^{-1} and 1020 cm^{-1} were assigned to the ν(O–H) stretching vibration and showed the existence of water molecules. The ν(N–C═O) stretching vibration absorption peaks also has been noticed around 2360 cm^{-1}. The vibration peaks around 1615 cm^{-1} ascribed to ν(C═N) stretching vibration absorption peak.

3.2. *Relative growth rate and ion homeostasis in nano Tb concentrations-treated Lemna minor*

Changes in relative growth rate (RGR) and ion contents of plants exposed to nano-size Tb treatments were given in Fig. 2. As shown in Fig. 2A, increments in relative growth rate (RGR) of 23% were seen in response to Tb-5 and Tb-10 treatments. In Tb-25 and Tb-50 applications, similar results to control levels were obtained. However, Tb treatments at high doses to *L. minor* resulted in significant RGR reductions in Tb-100, Tb-250 and Tb-500 groups. The endogenous accumulation of Tb increased in *L. minor* depending on Tb concentrations in the experimental groups (Fig. 2B). The maximum endogenous content of Tb was observed under the highest nano-size TB application. Except for Fe content in the nano-size Tb-25 group, the endogenous ion contents increased under Tb-5 and Tb-100 concentrations. On the contrary, 500 mg L^{-1} nano-size Tb toxicity led to a decrease in K, Mg, S, Mn and Fe contents. With nano-size Tb toxicity, N and Ca content did not decrease at the same Tb treatment.

3.3. *Chlorophyll fluorescence in nano Tb concentrations-treated Lemna minor*

F_v/F_m decreased at higher concentrations, with no changes observed

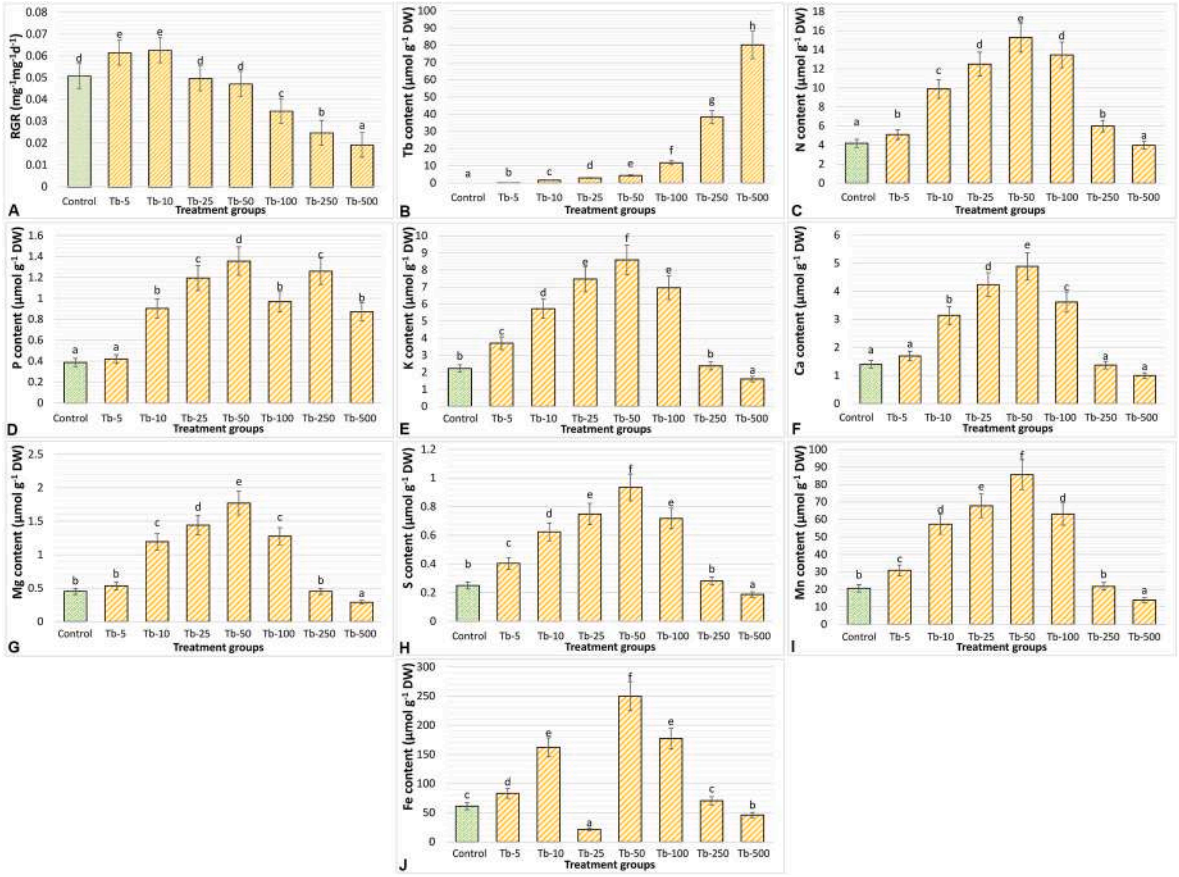

Fig. 2. The relative growth rate (RGR, **A**), the accumulation of nano-size Tb (**B**) and the contents of nitrogen (N, **C**), phosphate (P, **D**), potassium (K, **E**), calcium (Ca, **F**), magnessium (Mg, **G**), sulfur (S, **H**), manganase (Mn, **I**) and iron (Fe, **J**) in nano-size Tb-treated *L. minor*. Tb-5: 5 mg L^{-1}, Tb-10: 10 mg L^{-1}, Tb-25: 25 mg L^{-1}, Tb-50: 50 mg L^{-1}, Tb-100: 100 mg L^{-1}, Tb-250: 250 mg L^{-1}, Tb-500: 500 mg L^{-1} Tb.

up to nano-size Tb-100 concentration in plants which exposed to Tb treatments (Fig. 3A). As indicated in Fig. 3B, the similar trend was appeared in the F_v/F_o of *Lemna minor* subject to nano-size Tb. A significant decline in F_v/F_o was observed after Tb-250 and Tb-500 exposures. In contrast, the high concentrations of nano-size Tb (Tb-250 and Tb-500) led to an increase in F_o/F_m (Fig. 3C).

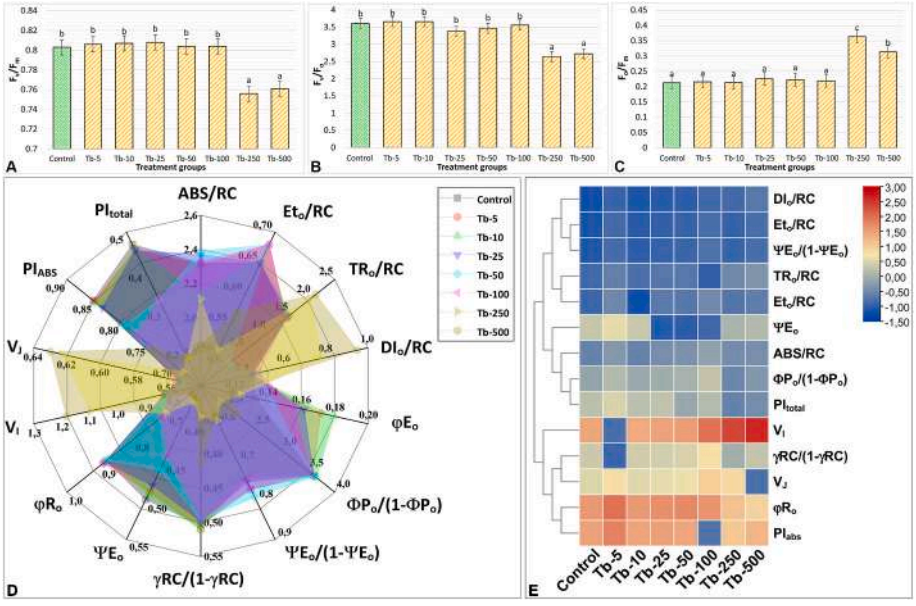

Fig. 3. The maximal quantum yield of PSII photochemistry (F_v/F_m, **A**), potential photochemical efficiency (F_v/F_o, **B**) and physiological state of the photosynthetic apparatus (F_o/F_m, **C**) in nano Tb-treated *L. minor*. The quantum efficiencies, structural indicators and fluxes and performance indices (**D**) and heat maps of treatment groups (log10-transformed TPM values (**E**) in *Lemna minor* under 5-10-25-50-100-250-500 mg L^{-1} Tb. The parameters derived from the portable fluorometer and OJIP transient and their definitions for use in the current study were given in Supplementary Table S1. The definition of groups was given in Fig. 2.

3.4. Fluorescence kinetics and performance of PSII in nano Tb concentrations-treated Lemna minor

Under low concentrations, Tb applications did not significantly alter the ABS/RC, ET_o/RC, TR_o/RC, $\Psi E_o/(1-\Psi E_o)$, $\Phi P_o/(1-\Phi P_o)$, γRC/(1-γRC), DI_o/RC, PI_{ABS} and PI_{total} values (Fig. 3D). When L. *minor* was exposed to 250 and 500 mg L^{-1} nano-size Tb, ABS/RC (light energy absorbed to reaction center) decreased. On the contrary, increased levels of DI_o/RC (scattering energy flux) and TR_o/RC (trapped energy flux per active PSII reaction center) detected (Fig. 3D). However, the low electron transfers in the reaction center of PSII indicated that ET_o/RC (electron transport flux) was reduced under high-dose Tb treatments. Likewise, the efficiency of the light reaction ΦPo/(1- ΦPo) and the performance index (PI_{total}) in the energy absorption pathway were declined. Fig. 3E represented that the levels of fluorescence-related parameters are depicted according to the color scale, where a change from blue to red indicates induction in these parameters from low to high levels.

3.5. Hormetic effect of nano Tb applications on H_2O_2 accumulation and lipid peroxidation in Lemna minor

H_2O_2 content and lipid peroxidation levels were shown in Fig. 4. While H_2O_2 content of *L. minor* did not change up to the Tb-100 concentration, the higher concentrations of nano-size Tb treatments (nano-size Tb-250 and Tb-500) induced this content (Fig. 4A). Likewise, a similar trend to H_2O_2 content was observed at higher doses for TBARS content, which was the same as control levels up to the nano-size Tb-100 concentration (Fig. 4B).

3.6. Hormetic effect of nano Tb applications on enzyme/isoenzyme activities in Lemna minor

As shown in Fig. 5A, seven bands (Mn-SOD1-2-3, Fe-SOD1-2 and Cu/Zn-SOD1-2) were observed for SOD isozymes in *L. minor*. Subject to nano-size Tb treatments increased total SOD activities in all treatment groups compared to the control plants (Fig. 5B). This increase in SOD activity was based on Mn-SOD2-3. All Tb applications had only one CAT isoform (Fig. 5C). Consistent with the intensity of the CAT isoform, total CAT activities increased up to Tb-100 concentration, while the similar activity to the control level was detected under Tb-250 and Tb-500 (Fig. 5D). The highest increase in CAT activity was seen in the Tb-100 group with approximately 3.4 times.

Fig. 6A showed that three bands (POX1-2-3) were identified during the experimental period in *L. minor*. In the Tb-5, Tb-10, Tb-25 and Tb-50 groups, increases in POX activities were detected in parallel with the induced intensities of all isozymes (Fig. 6B). *L. minor*, which had similar activities to control levels under Tb-100 and Tb-250, showed a decrease in POX activity in the Tb-500 group. Three bands (NOX1-2-3) were observed for NOX isoforms throughout the experimental period (Fig. 6C). Tb exposure resulted in significant increases in total NOX activities up to Tb-100 concentration (Fig. 6D). While NOX activity in the Tb-250 group was similar to the control level, a decrease was measured at the highest dose (Tb-500). As seen in Fig. 6C, these changes were evidenced by NOX2-3 intensities.

The changes in GST isoforms (GST1-2-3-4) consisting of four bands in *L. minor* were illustrated in Fig. 7A. There were noticeable increases in total GST activities up to Tb-100 administration (Fig. 7B). In contrast, a reduction of approximately 42% was seen in the Tb-250 group compared to the control. No remarkable change was detected in the Tb-500 group. All isoforms were responsible for these changes. The three bands (GPX1-2-3) detected for the GPX isoforms were shown in Fig. 7C. Exposure to Tb showed a similar trend in GPX activities to GST activities (Fig. 7D).

3.7. Hormetic effect of nano Tb applications on enzyme/isoenzyme activities related to AsA-GSH cycle in Asada-Halliwel pathway of Lemna minor

Specification of APX isoenzymes of *L. minor* revealed seven isoforms (APX1-2-3-4-5-6-7) (Fig. 8A). All Tbs, except for Tb-250 and Tb-500, significantly increased APX activity (Fig. 8B). The maximum induction was under Tb-100 treatment in APX with 76.4%. APX activities were decreased in the plants treated with Tb-250 and Tb-500 compared to the control. These trends were due to the intensities of APX1-4-7. As shown in Fig. 8C, *L. minor* had five bands (GR1-2-3-4-5) for the GR isozymes. In a similar manner to APX activity, all Tb treatments increased GR activities, except for Tb-250 and Tb-500 (Fig. 8D). In the Tb-250 and Tb-500 groups, it was similar to the control level. GR isozyme analysis showed that GR1-2-4 isoforms were responsible for the changes in GR activities.

In *L. minor* exposed to Tb, the increased MDHAR activities were observed in direct proportion to increasing Tb concentrations (Fig. 9A). There was an increase in DHAR activity in all groups except Tb-250 and Tb-500. DHAR activity of the Tb-250 group was similar to the control level, while it was lower than the control level in Tb-500 (Fig. 9B). Tb applications to *L. minor* resulted in increased levels of total AsA content up to the Tb-50 concentration. At higher concentrations, however, AsA content was markedly reduced (Fig. 9C). In return for Tb, DHA content showed an increase only in the Tb-500 group during the experiment period while it decreased in all other treatments (Fig. 9D). The increased GSH content up to the Tb-50 group decreased at higher doses. GSH content was similar to the control level in the Tb-100 and Tb-250 groups but it was approximately 30% less than the control level under Tb-500 (Fig. 9E). In contrast to the GSH content, GSSG contents tended to decrease up to the Tb-50 group. Conversely, the induced GSSG contents were detected at higher Tb concentrations (Tb-100-250-500) (Fig. 9F). Depending the determination of total ascorbate (tAsA) and DHA contents, AsA/DHA rates increased only in exposure to Tb-5-10-25-50 (Fig. 9G). Significant reductions in GSH redox status were found with Tb-100-250-500 applications to *L. minor* compared to control groups (Fig. 9H).

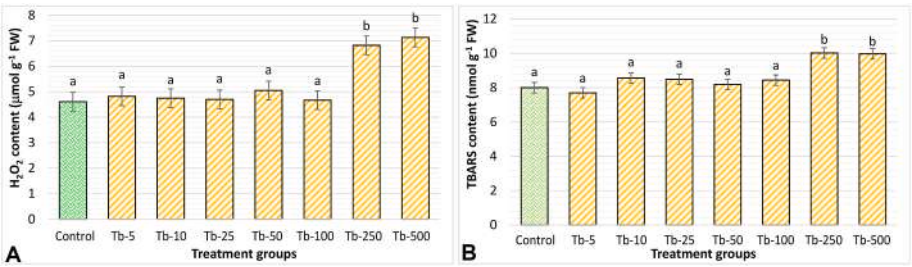

Fig. 4. Hydrogen peroxide (H_2O_2, **A**) and lipid peroxidation (TBARS, **B**) levels in nano Tb-treated *L. minor*. The definition of groups was given in Fig. 2.

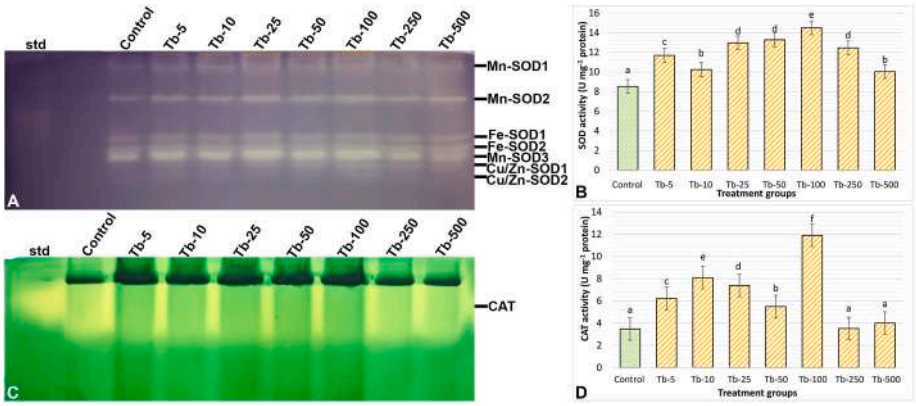

Fig. 5. Relative band intensity of different types of superoxide dismutase isoenzymes (SOD, **A**) and SOD activity (**B**), relative band intensity of different types of catalase isoenzymes (CAT, **C**) and CAT activity (**D**) in nano Tb-treated *L. minor*. The definition of groups was given in Fig. 2.

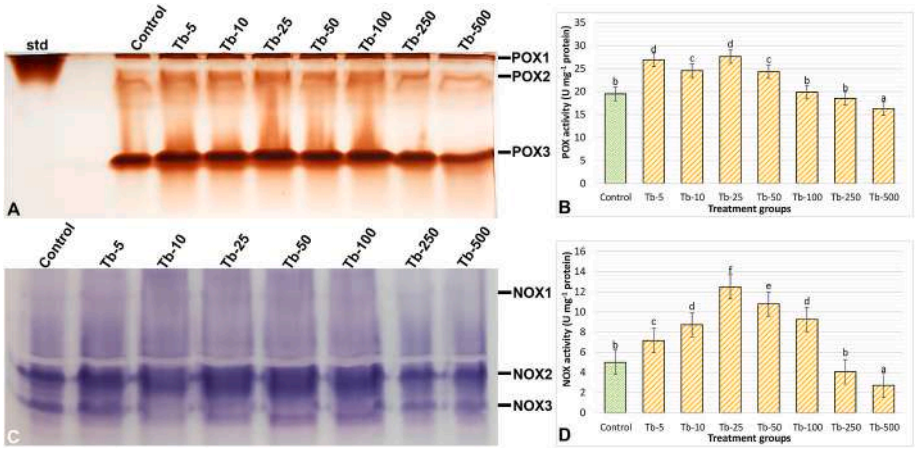

Fig. 6. Relative band intensity of different types of peroxidase isoenzymes (POX, **A**) and POX activity (**B**), relative band intensity of different types of NADPH oxidase isoenzymes (NOX, **C**) and NOX activity (**D**) in nano Tb-treated *L. minor*. The definition of groups was given in Fig. 2.

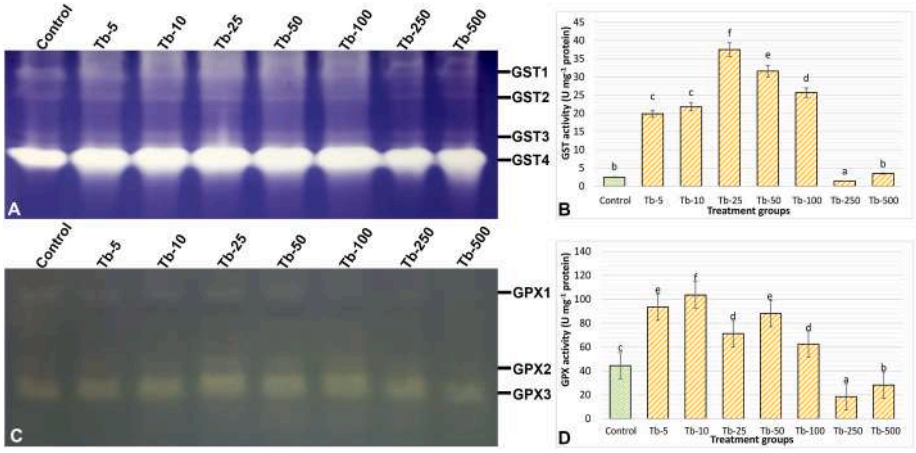

Fig. 7. Relative band intensity of glutathione *S*-transferase isoforms (GST, **A**), GST activity (**B**), relative band intensity of different types of glutathione peroxidase isoenzymes (GPX, **C**) and GPX activity (**D**) in nano Tb-treated *L. minor*. The definition of groups was given in Fig. 2.

3.8. Hormetic effect of nano Tb applications on hormone contents in Lemna minor

As seen in Fig. 10A, increased indole-3-acetic acid (IAA) contents were detected up to the Tb-100 group. The high dose groups (Tb-250 and Tb-500) had unchanged IAA contents compared to the control. As illustrated in Fig. 10B, abscisic acid (ABA) content was reduced by approximately 33% in *L. minor* treated with Tb-5. On the other hand, ABA contents showing similar amounts to control levels in Tb-10-25-50 groups were induced at higher Tb concentrations (Tb100-250-500). The results presented in Fig. 10C revealed that Tb-10-25-50-100 increased the gibberellic acid (GA) content in *L. minor* compared to the control

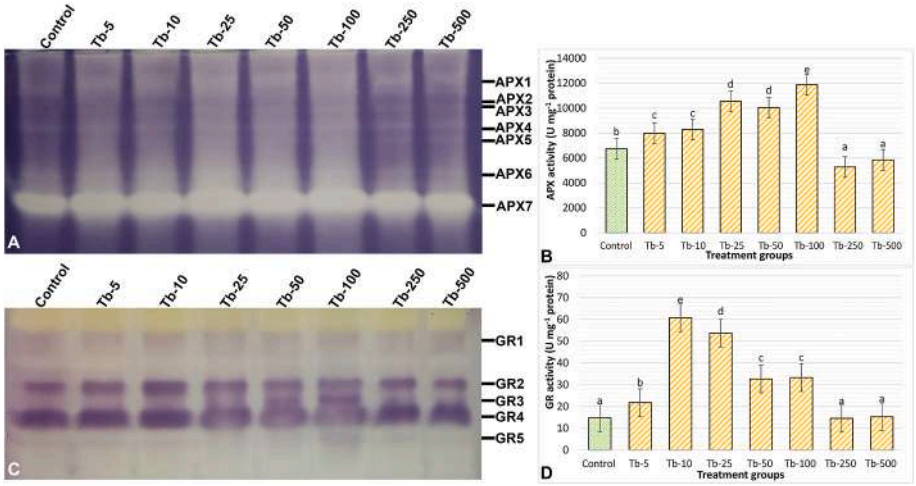

Fig. 8. Relative band intensity of ascorbate glutathione (APX, **A**), APX activity (**B**), relative band intensity of glutathione reductase isoenzymes (GR, **C**) and GR activity (**D**) in nano Tb-treated *L. minor*. The definition of groups was given in Fig. 2.

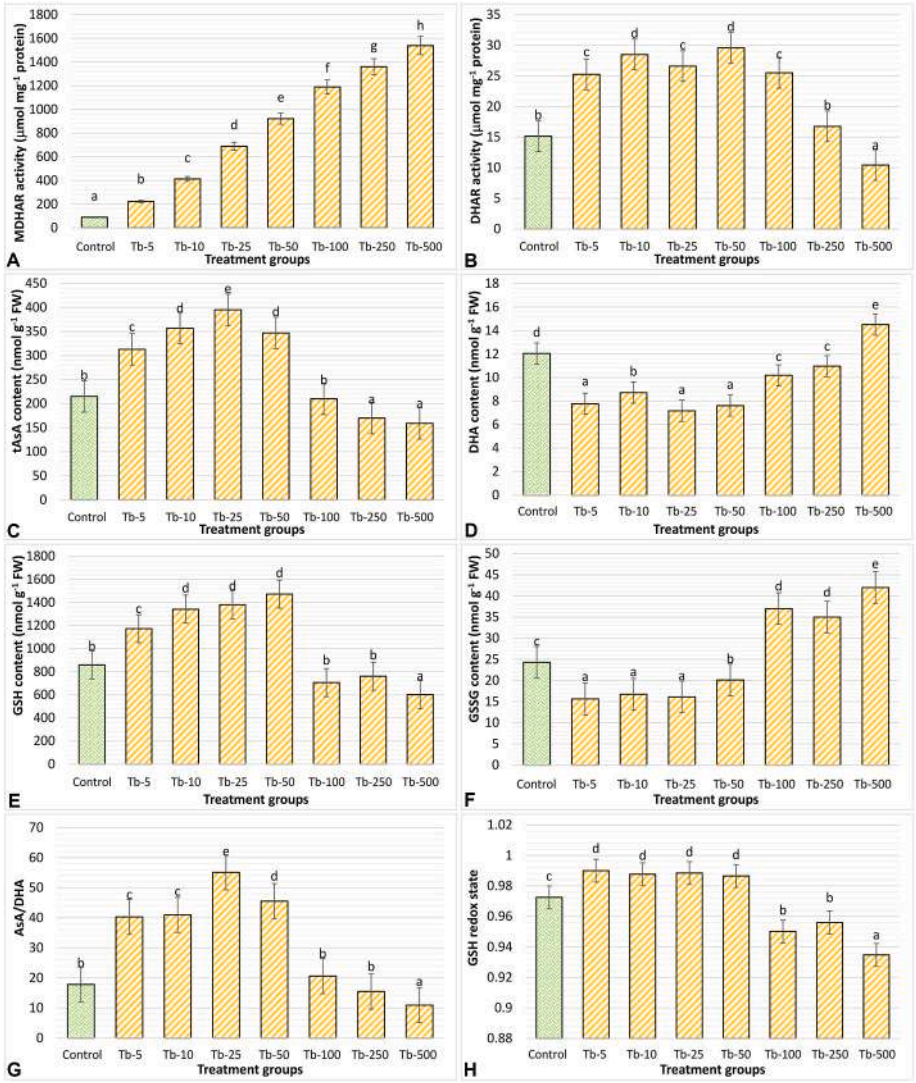

Fig. 9. The monodehydroascorbate reductase activity (MDHAR, **A**), dehydroascorbate reductase activity (DHAR, **B**), ascorbate content (tAsA, **C**), dehydroascorbate content (DHA, **D**), glutathione content (GSH, **E**), oxidized glutathione content (GSSG, **F**), tAsA/DHA (**G**) and GSH redox state (**H**) in nano Tb-treated *L. minor*. The definition of groups was given in Fig. 2.

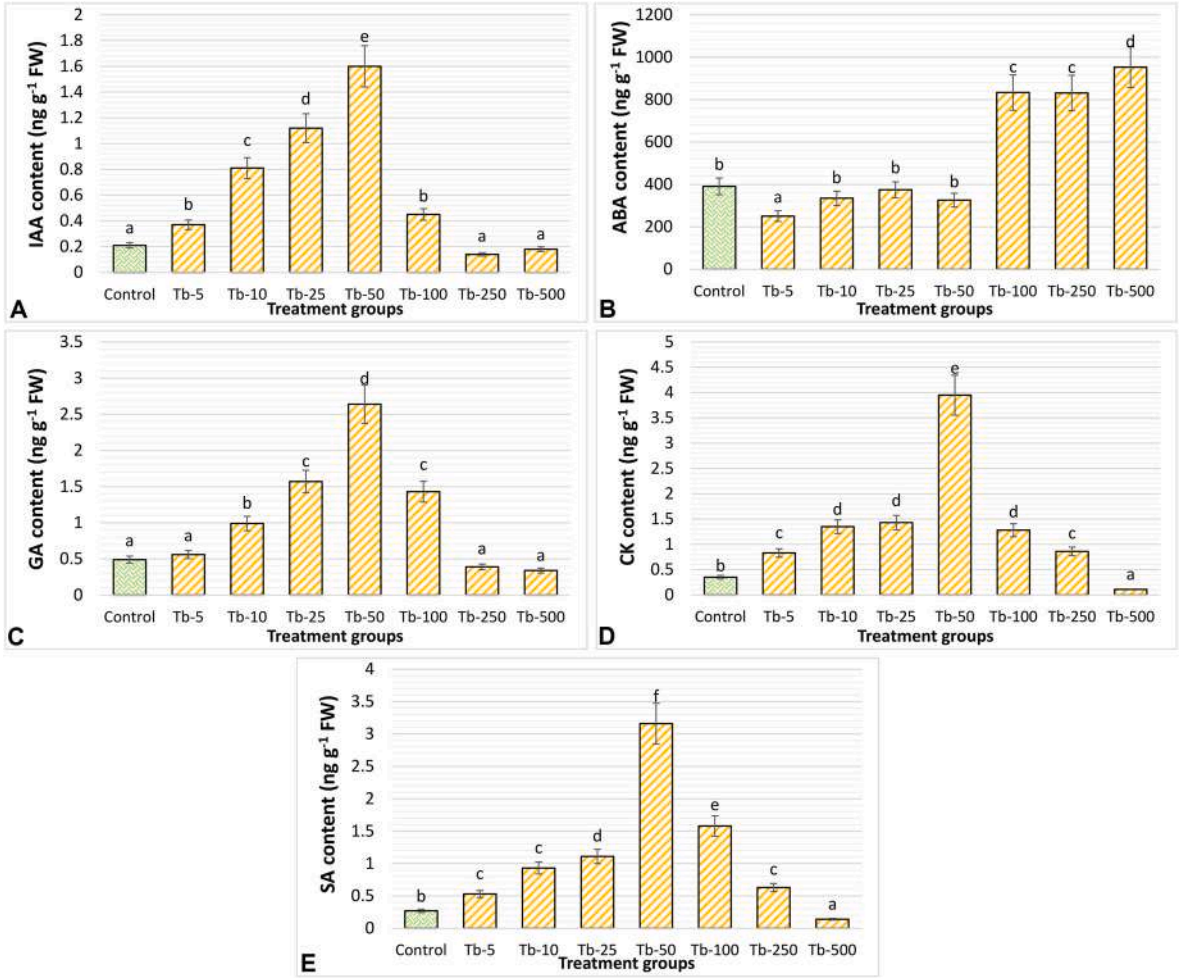

Fig. 10. The contents of indole-3-acetic acid (IAA, **A**), abscisic acid (ABA, **B**), Gibberellic acid (GA, **C**), cytokinin (CK, **D**), salicylic acid (SA, **E**) in nano Tb-treated *L. minor*. The definition of groups was given in Fig. 2.

plants. The highest increase was seen in the Tb-50 group with approximately 5.4 times. Likewise, Tb exposure in *L. minor* resulted in significantly increased cytokinin (CK) contents in all groups, except for Tb-500. In contrast, CK content in Tb-500-applied plants was approximately 3 times less (Fig. 10D). Similar trend to CK content was also detected in the results of salicylic acid (SA) contents. The highest increase was seen in the Tb-50 plants with approximately 11.7-fold (Fig. 10E).

4. Discussion

According to SEM images, the control plant sample did not include the nanocrystalline Tb_4O_7 indicated by the red arrows in Fig. 1C. This proved that, as shown in Fig. 1C, Tb_4O_7 NPs primarily permeated the plant sample. The morphologies of the plant samples prepared with and without the addition of nanocrystalline Tb_4O_7 were evaluated by SEM–EDX analysis (Fig. 1F). The proper SEM-EDX spectrum was used to determine the samples' contents. The plant sample without Tb_4O_7 NPs had no Tb content, unlike the plant samples containing Tb_4O_7 NPs, as depicted in Fig. 1F. In that respect, the synthesized Tb_4O_7 nanosheets in plant samples were identified by SEM–EDX analysis. When the FT-IR spectra of the plant samples included with Tb_4O_7 NPs were analyzed, it has detected that the intensities were higher than the control plant sample. Consequently, it was concluded that Tb_4O_7 NPs were successfully incorporated into the structure of the plant samples. At this stage, when the control plant sample and the Tb_4O_7 NPs integrated plant sample were compared, peak shifts were observed in the FTIR spectrum of dopant appear in the plant sample. It can be seen that the nitrogen atom of the C═N group is coordinated to the terbium (III) ions by the red shift of the ν (C═N) stretching vibration absorption peak from 1615 cm^{-1}–1612 cm^{-1}. Additionally, the red shift of the ν (N–C═O) stretching vibration absorption peak from 2357 cm^{-1}–2355 cm^{-1} indicated that the oxygen atom of the N–C═O group had coordinated to the terbium(III) ions (Xiao et al., 2019).

In recent years, negative, positive or no effects of REE on plant growth have been observed around the world. Previous studies show that low concentrations of REE stimulate growth, whereas high doses of REE inhibit growth (Kovaříková et al., 2019). On the other hand, nanoparticle form of Tb donors has emerged as a strategy that could protect these molecules from decomposition/degradation and allow a controlled Tb release. Also, nanoparticles present distinct physico-chemical characteristics compared to the same material at the macroscopic scale, with an increase in the superficial area (Oliveira et al., 2016). In the present study, the Tb nanoparticle application had a beneficial effect by improving the growth of *L. minor* when supplied in appropriate concentrations. However, an excess of Tb caused toxicity and reduced plant growth. The beneficial effects may be due to the stimulatory effects of Tb on nutrient uptake by plants and/or the increased synthesis of chlorophyll in the plant (Xu and Wang, 2007). Photosystem II (PSII) is a pigment-protein compound that combines various carriers of the electron transport chain (ETC) in photosynthetic processes in plants. The oxygen-evolving centers (OEC) in this PSII are vital biological clusters of Mn_4CaO_5 that catalyzes the water splitting reaction (Yao et al., 2021). In this present study, exposure to 5–100 mg

L^{-1} Tb did not decrease PSII activity, while an increase was detected in the F_o/F_m ratios of the groups treated with high Tb doses. A decrease was detected in the F_v/F_m and F_v/F_o in Tb-250 and Tb-500 treated plants, which state the maximum primary photochemistry efficiency of PSII. This indicates that electron transport is slowed between primary (Q_A) and secondary (Q_B) quinones at the acceptor side of PSII (Gupta et al., 2021). Chlorophyll fluorescence analyzes, which are considered to be the most sensitive parameters of plant photosynthetic capacity, showed that Tb toxicity inactivated the performance of reaction centers in PSII, causing a decrease in photosynthetic capacity. On the other hand, considerable amounts of N, Mg and other elements are required for the biosynthesis of chlorophyll precursors. Low Tb doses may enhance the absorption of these elements, resulting in an increment in chlorophyll contents. When *G. lucidum* was cultivated with different concentrations of REEs (25, 50, 100, 150, 200 and 250 μg g^{-1}), change of the contents of other minerals was observed in the plant tissues (Zhang et al., 2013). REEs regulate plant growth by affecting the contents of mineral elements such as K, Ca, Mg, Fe (Hu et al., 2002). In addition, it is possible that low REE doses affect the membrane potential and proton transmembrane gradient by promoting photosynthesis (Cheng et al., 2021). A number of studies revealed that several REEs play several catalytic roles in chlorophyll formation and indirectly contribute to chlorophyll biosynthesis (Hong et al., 2002). At high doses, it can replace Mg^{2+} and Fe^{2+} to form a terbium-chlorophyll in the chloroplast complex (Song et al., 2002). Likewise, as the terbium concentration in *L. minor* increases, non-functional replacement of Ca^{2+} with a competitive terbium ion in the OEC may occur (Loktyushkin et al., 2019). But in fact, Ca^{2+} is a required cofactor for the water oxidation reaction and modulates the redox potential of the manganese cluster (Mn_4CaO_5) of the D1 protein in the center of PSII (Shamsipur and Pashabadi, 2018). Similar to these results, it was revealed that high doses of REEs cause PSII inhibition (Yao et al., 2021).

Chlorophyll fluorescence can be used to analyze detailed information about energy transfer in photosynthesis. A descriptive tool for providing information about the state of PSII, the OJIP test relies on rapid kinetic analysis of chlorophyll fluorescence and signals that provide detailed information about the structure and function of the photosynthetic apparatus (Sameena and Puthur, 2021). To assess the hormetic effect of Tb in PSII, alterations in electron transport reduction and various phenomenological fluxes (ABS/RC, TR_o/RC, ET_o/RC, and DI_o/RC) were measured. Results showed that Tb treatments at low doses induced or did not change these rates suggesting that REEs could enhance the efficiency of light absorption, regulate excitation energy distribution from photosystem I (PSI) to PSII, and thus increase the activity of photochemical reaction and oxygen evolution accordingly. Xiaoqing et al. (2009) reported that the PSII efficiency of the Ce^3, Nd^3 and La^3 treatments was higher than the control in *A. thaliana*. In the current study, DI_o/RC increased as ET_o/RC decreased in *L. minor* treated with high doses of Tb. Such effects can result from damage to the PSII. On the other hand, quantum efficiency, energy flows for absorption and capture, electron transport and energy dissipation flows showed that the energy capture, transport and termination efficiency of *L. minor* were low. This means that Tb toxicity decreased the transfer and utilization of energy through light harvesting, light energy capture and electron transport. At the same time, excess Tb increased TR_o/RC followed by a decrease in Q_A. The reducement in ΨE_o, φP_o and φR_o, which is related to quantum efficiency, demonstrated the declined electron flux in PSII. This kind of reductions was indicative for the electron transfer from primer quinone acceptor Q_A^- to secondary quinone acceptor Q_B and reduction of acceptor side of PSI downregulated in high dose Tb-exposed *L. minor*. However, when interpreted results of $\Phi P_o/(1\text{-}\Phi P_o)$, $\Psi E_o/(1\text{-}\Psi E_o)$ and $\gamma RC/(1\text{-}\gamma RC)$, Tb adversely affected the trapped energy by active reaction centers and transport to the end electron acceptors at photosystem I (PSI). The disruptions in all relevant data realized in the photosynthesis performance indices (PI_{total} and PI_{ABS}), are conformable to earlier results in REE-treated plants (Loktyushkin et al., 2019).

The first line of defense against reactive oxygen species (ROS) caused by stress is the SOD enzyme, which catalyzes to convert superoxide anions into H_2O_2, followed by CAT and POX. In addition, the activity of NADPH oxidase (NOX) is evaluated as an important resource of a considerable amount of superoxide radical and H_2O_2 in plants (Chu--Puga et al., 2019). Due to the activities of SOD and NOX, increased levels of H_2O_2 induced TBARS content. Therefore, increases in H_2O_2 and TBARS levels can be an acceptable indicator of oxidative stress in plant cells (Rajput et al., 2021). In the current study, exposure up to 100 mg L^{-1} nano-size Tb did not change H_2O_2 and TBARS levels, while these contents were induced at higher doses (250 and 500 mg L^{-1}) compared with control. This indicates the toxic effect of high doses of Tb applications in *L. minor*. Similar concentration-dependent effects of REEs have been previously detected in several plants (Agathokleous et al., 2018). It has been revealed that the increase in SOD activity is associated with the augmented tolerance of plants to abiotic stress (Berwal and Ram, 2018). In this study, low doses of Tb applications induced SOD, CAT and POX activities in *L. minor*. On the contrary, at high doses, CAT and POX activities decreased, while SOD activity was higher than that of the control group. This may be attributed to the accumulated levels of H_2O_2 and TBARS in the high-dose Tb treated groups (Tb-250-500). Similarly, Dridi et al. (2022) found that REE applications increased the SOD activity in *Helianthus annuus*. The results are similar to the study showing that excessive REE concentrations inhibit CAT and POX activities, while low concentrations of REEs promote antioxidant enzyme activity (Fan et al., 2020).

H_2O_2 is converted to non-radical formations by the Asada-Halliwell pathway involved enzyme system (AsA-GSH cycle) simultaneously with CAT and POX enzymes (Rajput et al., 2021). In the AsA-GSH cycle, the coordinated functions of APX, MDHAR, DHAR and GR along with AsA and GSH split H_2O_2 into water and oxygen and recycle AsA and GSH. The maintaining of high AsA/DHA and/or GSH/GSSG conferred by increased AsA and GSH or reduced DHA and GSSG may be the main strategy for defense against abiotic stress-induced ROS accumulation (Shan et al., 2020). In the present study, low-dose Tb applications resulted in high AsA and GSH content in *L. minor*. Due to increased APX, GR, MDHAR and DHAR activities, high rates of AsA/DHA and GSH/GSSG, the pool of AsA and GSH, and the unsuppressed GSH redox state were maintained. In addition, the increased activities of GST and GPX, depending on the preserved GSH levels, could also contribute to preventing the accumulation of H_2O_2. This resulted in unchanged levels of H_2O_2 and TBARS in comparison of the control plants. Owing to this enhancement in the antioxidant system could not be sustained after higher doses of Tb treatments (Tb250- and Tb500), TBARS and H_2O_2 contents increased. These hormetic effects of Tb obtained in the current study were also detected in *Salvia miltiorrhiza*, which was exposed to increased REE applications (Fan et al., 2020). The dose dependents effects of La^{3+} on *L. minor* and cucumber seedlings have also been reported (Ippolito et al., 2011; Paola et al., 2007).

Numerous recent research has proven that phytohormones such auxin (as indole-3-acetic acid-IAA), cytokinin (CK), salicylic acid (SA) and gibberellic acid (GA) work in combination with the central hormone abscisic acid (ABA) or with each other to regulate plant responses under stress conditions (Mubarik et al., 2021). Furthermore, high endogenous auxin (IAA), GA, CK and SA levels are associated with triggering the expression of some stress-related genes and the activity of ROS detoxifying enzymes (Salvi et al., 2021). In the presence of abiotic stress conditions, ABA biosynthesis and its accumulation in some plant tissues are greatly increased and binds to its receptors to trigger signal transduction that results in the stress response at the cellular level. As stress signals emerge, ABA level in the plant system increases and triggers the expression of stress tolerance-related genes (Rachappanavar et al., 2022). In the current study, H_2O_2 contents were similar to control levels in *L. minor* exposed to low Tb doses. Therefore, ABA contents at control levels can be attributed to unstressed plant metabolism. Under abiotic stress conditions, the crosstalk between ABA and IAA helps seeds

survive, and ABA modulates IAA transport to sustain growth. In addition, APX has been identified as an enzyme that mediates the crosstalk between ABA, IAA and ROS to protect plants from oxidative damage (Chen et al., 2014). It is unraveled that there is an antagonistic crosstalk between GA and ABA regulated by the same DELLA proteins. This mechanism allows plants to recover from stress conditions by prolongationing seed dormancy (Chen et al., 2020). The crosstalk between ABA and SA helps to maintain water status in plants and regulate stomatal conductivity and osmotic regulation (Khan et al., 2020). ABA and CK have an antagonistic role in the control of stomatal function under stress conditions (Jogawat, 2019). The application of low Tb concentrations increased the content of these phytohormones. Similarly, in *D. densiflorum*, 5 μM Nd^{3+} significantly increased the endogenous IAA level and the ratio of IAA to cytokinins (CKs) during the process of root primordium formation, which may favor adventitious rooting of *D. densiflorum* shoot cuttings (Jianping et al., 2008). Also, in wheat seedlings, low doses of $La(NO_3)_3$ can increase the level of hormone contents (Yang et al., 2006). On the other hand, low doses of Tb treatments strengthened the defense system in *L. minor* together with the induced antioxidant system activity, as evident from the constant H_2O_2 and TBARS level. Fashui et al. (2003) reported REE and antioxidant-phytohormone relationships. The results obtained are related to the fact that antioxidant system-related phytohormone production is affected by the presence of Tb and this effect is especially related to the synergistic effect of REEs with hormones (Hu et al., 2004; Ramos et al., 2016). At high doses, the increase in ABA contents due to increased H_2O_2 accumulation was a sign that Tbs administered at high doses showed toxic properties. On the other hand, the reason why the toxicity could not be eliminated despite the increased ABA content was insufficient IAA, GA, CK and SA contents and thus decreased antioxidant system activity.

5. Conclusion

Depending on Tb concentrations, Tb altered the endogenous ion contents of *L. minor*. The low concentrations of Tb induced the ion uptake, and the high Tb treatments (especially Tb250- and Tb-500) caused a reduction in ion accumulation. On the other hand, excessive Tb treatments caused a decrease in the photosynthetic efficiency and chlorophyll fluorescence of *L. minor*. At low doses, however, these parameters were similar to the control and no adverse effects of photosystems were observed. Tb5-10-25-50 did not change in H_2O_2 and TBARS contents by inducing SOD, CAT, POX, GST, and GPX and maintaining a high AsA/DHA and GSH redox state. Thus, the regeneration of AsA and GSH contributed to the inhibition of oxidative damage. Besides, at appropriate concentrations, Tb can protect the plant against stress by inducing their hormone contents. Interestingly, despite the inactivated AsA-GSH cycle, Tb-100 could protect from the radical accumulation-triggered damage by activating SOD and CAT enzymes. On the other hand, under Tb-250 and Tb-500, H_2O_2 accumulation was triggered and then lipid peroxidation was induced due to insufficient antioxidant capacity and hormone contents. The treatment of 5–100 mg L^{-1} nano-size Tb has great potential to confer tolerance of duckweed by supporting the antioxidant system, protecting the biochemical reactions of photosystems and improving hormonal regulation.

CRediT authorship contribution statement

E.Y. and C.O.K. designed experiments; B.A., F.N.A., E.Y., C.G. and C. O.K. carried out data analysis; H.C., TB characterization; M.T., TB content; F.N.A., C.O.K. and E.Y. interpreted the results and wrote up the first draft of the manuscript; C.O.K. and E.Y. critically edited the whole manuscript. All authors read and approved the final manuscript.

Declaration of competing interest

The authors declare that they have no known competing financial interests or personal relationships that could have appeared to influence the work reported in this paper.

Data availability

The authors do not have permission to share data.

Appendix A. Supplementary data

Supplementary data to this article can be found online at https://doi.org/10.1016/j.plaphy.2022.11.031.

References

Agathokleous, E., Kitao, M., Calabrese, E.J., 2018. The rare earth element (REE) lanthanum (La) induces hormesis in plants. Environ. Pollut. 238, 1044–1047. https://doi.org/10.1016/j.envpol.2018.02.068.

Agathokleous, E., Kitao, M., Calabrese, E.J., 2019. Hormesis: a compelling platform for sophisticated plant science. Trends Plant Sci. 24, 318–327. https://doi.org/10.1016/j.tplants.2019.01.004.

Basiglini, E., Pintore, M., Forni, C., 2018. Effects of treated industrial wastewaters and temperatures on growth and enzymatic activities of duckweed (*Lemna minor* L.). Ecotoxicol. Environ. Saf. 153, 54–59. https://doi.org/10.1016/j.ecoenv.2018.01.053.

Battal, P., Tilekliioglu, B., 2001. The effects of different mineral nutrients on the levels of cytokinins in maize (*Zea mays* L.). Turk. J. Bot. 25, 123–130.

Beauchamp, C., Fridovich, I., 1971. Superoxide dismutase: improved assays and an assay applicable to acrylamide gels. Anal. Biochem. 44, 276–287. https://doi.org/10.1016/0003-2697(71)90370-8.

Bergmeyer, H.U., 1970. Methoden der enzymatischen Analyse. 2. Verlag Chemie. https://doi.org/10.1002/pauz.19750040306.

Berwal, M., Ram, C., 2018. Superoxide dismutase: a stable biochemical marker for abiotic stress tolerance in higher plants. Abiotic and Biotic Stress in Plants 1–10. https://doi.org/10.5772/intechopen.82079.

Bradford, M.M., 1976. A rapid and sensitive method for the quantitation of microgram quantities of protein utilizing the principle of protein-dye binding. Anal. Biochem. 72, 248–254. https://doi.org/10.1016/0003-2697(76)90527-3.

Cao, Z., Stowers, C., Rossi, L., Zhang, W., Lombardini, L., Ma, X., 2017. Physiological effects of cerium oxide nanoparticles on the photosynthesis and water use efficiency of soybean (*Glycine max* (L.) Merr.). Environ. Sci. Nano 4, 1086–1094. https://doi.org/10.1039/C7EN00015D.

Cheeseman, J.M., 2006. Hydrogen peroxide concentrations in leaves under natural conditions. J. Exp. Bot. 57, 2435–2444. https://doi.org/10.1093/jxb/erl004.

Cheikh, N., Jones, R.J., 1994. Disruption of maize kernel growth and development by heat stress (role of cytokinin/abscisic acid balance). Plant Physiol. 106, 45–51. https://doi.org/10.1104/pp.106.1.45.

Chen, C., Letnik, I., Hacham, Y., Dobrev, P., Ben-Daniel, B.H., Vanková, R., Amir, R., Miller, G., 2014. Ascorbate Peroxidase6 protects *Arabidopsis* desiccating and germinating seeds from stress and mediates cross talk between reactive oxygen species, abscisic acid, and auxin. Plant Physiol. 166, 370–383. https://doi.org/10.1104/pp.114.245324.

Chen, H., Ruan, J., Chu, P., Fu, W., Liang, Z., Li, Y., Tong, J., Xiao, L., Liu, J., Li, C., 2020. AtPER1 enhances primary seed dormancy and reduces seed germination by suppressing the ABA catabolism and GA biosynthesis in *Arabidopsis* seeds. Plant J. 101, 310–323. https://doi.org/10.1111/tpj.14542.

Cheng, J., Du, X., Long, H., Zhang, H., Ji, X., 2021. The effects of exogenous cerium on photosystem II as probed by in vivo chlorophyll fluorescence and lipid production of *Scenedesmus obliquus* XJ002. Biotechnol. Appl. Biochem. 68, 1216–1226. https://doi.org/10.1002/bab.2043.

Chu-Puga, Á., González-Gordo, S., Rodríguez-Ruiz, M., Palma, J.M., Corpas, F.J., 2019. NADPH oxidase (Rboh) activity is up regulated during sweet pepper (*Capsicum annuum* L.) fruit ripening. Antioxidants 8, 9. https://doi.org/10.3390/antiox8010009.

Cutting, J.G., 1991. Determination of the cytokinin complement in healthy and witchesbroom malformed proteas. J. Plant Growth Regul. 10, 85–89. https://doi.org/10.1007/BF02279317.

d'Aquino, L., De Pinto, M.C., Nardi, L., Morgana, M., Tommasi, F., 2009. Effect of some light rare earth elements on seed germination, seedling growth and antioxidant metabolism in *Triticum durum*. Chemosphere 75, 900–905. https://doi.org/10.1016/j.chemosphere.2009.01.026.

Dridi, N., Brito, P., Bouslimi, H., Ferreira, R., Martins Dias, S., Caçador, I., Sleimi, N., 2022. Physiological and biochemical behaviours and antioxidant response of *Helianthus annuus* under lanthanum and cerium stress. Sustainability 14, 4153. https://doi.org/10.3390/su14074153.

Dutilleul, C., Driscoll, S., Cornic, G., De Paepe, R., Foyer, C.H., Noctor, G., 2003. Functional mitochondrial complex I is required by tobacco leaves for optimal photosynthetic performance in photorespiratory conditions and during transients. Plant Physiol. 131, 264–275. https://doi.org/10.1104/pp.011155.

Fan, Z., Zhang, K., Wang, F., Zhao, X., Bai, R., Liu, B., 2020. Effects of rare earth elements on growth and determination of secondary metabolites under in vitro conditions in *Salvia miltiorrhiza*. Hortscience 55, 310–316. https://doi.org/10.21273/HORTSCI14661-19.

Fashui, H., Ling, W., Chao, L., 2003. Study of lanthanum on seed germination and growth of rice. Biol. Trace Elem. Res. 94, 273–286. https://doi.org/10.1385/BTER:94:3:273.

Gupta, R., Sharma, R.D., Rao, Y.R., Siddiqui, Z.H., Verma, A., Ansari, M.W., Rakwal, R., Tuteja, N., 2021. Acclimation potential of Noni (*Morinda citrifolia* L.) plant to temperature stress is mediated through photosynthetic electron transport rate. Plant Signal. Behav. 16, 1865687 https://doi.org/10.1080/15592324.2020.1865687.

Gwenzi, W., Mangori, L., Danha, C., Chaukura, N., Dunjana, N., Sanganyado, E., 2018. Sources, behaviour, and environmental and human health risks of high-technology rare earth elements as emerging contaminants. Sci. Total Environ. 636, 299–313. https://doi.org/10.1016/j.scitotenv.2018.04.235.

Hernandez-Miñana, F.M., 1991. Identification of cytokinins and the changes in their endogenous levels in developing *Citrus sinensis* leaves. J. Hortic. Sci. 66, 505–511. https://doi.org/10.1080/00221589.1991.11516180.

Herzog, V., Fahimi, H., 1973. Determination of the activity of peroxidase. Anal. Biochem. 55, e62.

Hong, F., Wang, L., Meng, X., Wei, Z., Zhao, G., 2002. The effect of cerium (III) on the chlorophyll formation in spinach. Biol. Trace Elem. Res. 89, 263–276. https://doi.org/10.1385/BTER:89:3:263.

Hossain, M., Hossain, M., Fujita, M., 2006. Induction of pumpkin glutathione *S*-transferases by different stresses and its possible mechanisms. Biologia Plant 50, 210–218. https://doi.org/10.1007/s10535-006-0009-1.

Hu, H., Wang, L., Zhou, Q., Huang, X., 2016. Combined effects of simulated acid rain and lanthanum chloride on chloroplast structure and functional elements in rice. Environ. Sci. Pollut. Res. 23, 8902–8916. https://doi.org/10.1007/s11356-015-5962-9.

Hu, X., Ding, Z., Chen, Y., Wang, X., Dai, L., 2002. Bioaccumulation of lanthanum and cerium and their effects on the growth of wheat (*Triticum aestivum* L.) seedlings. Chemosphere 48, 621–629. https://doi.org/10.1016/S0045-6535(02)00109-1.

Hu, Z., Richter, H., Sparovek, G., Schnug, E., 2004. Physiological and biochemical effects of rare earth elements on plants and their agricultural significance: a review. J. Plant Nutr. 27, 183–220. https://doi.org/10.1081/PLN-120027555.

Hunt, R., Causton, D.R., Shipley, B., Askew, A.P., 2002. A modern tool for classical plant growth analysis. Ann. Bot. 90, 485–488. https://doi.org/10.1093/aob/mcf214.

Ion, R.M., Sorescu, A.A., Nuta, A., 2021. Green synthesis of lanthanides and actinides-based nanomaterials. In: Kharisov, B., Kharissova, O. (Eds.), Handbook of Greener Synthesis of Nanomaterials and Compounds. Elsevier, pp. 355–388.

Ippolito, M., Fasciano, C., d'Aquino, L., Tommasi, F., 2011. Responses of antioxidant systems to lanthanum nitrate treatments in tomato plants during drought stress. Plant Biosyst. 145, 248–252. https://doi.org/10.1080/11263504.2010.509937.

Jiang, M., Zhang, J., 2002. Involvement of plasma-membrane NADPH oxidase in abscisic acid- and water stress-induced antioxidant defense in leaves of maize seedlings. Planta 215, 1022–1030. https://doi.org/10.1007/s00425-002-0829-y.

Jianping, L., Zhang, J., Ying, W., 2008. Changes in endogenous hormone levels and redox status during enhanced adventitious rooting by rare earth element neodymium of *Dendrobium densiflorum* shoot cuttings. J. Rare Earths 26, 869–874. https://doi.org/10.1016/S1002-0721(09)60023-5.

Jogawat, A., 2019. Crosstalk among phytohormone signaling pathways during abiotic stress. In: Roychoudhury, A., Tripathi, D. (Eds.), Molecular Plant Abiotic Stress: Biology and Biotechnology, pp. 209–220. https://doi.org/10.1002/9781119463665.ch11.

Khan, N., Bano, A., Ali, S., Babar, M., 2020. Crosstalk amongst phytohormones from planta and PGPR under biotic and abiotic stresses. Plant Growth Regul. 90, 189–203. https://doi.org/10.1007/s10725-020-00571-x.

Kovaříková, M., Tomášková, I., Soudek, P., 2019. Rare earth elements in plants. Biologia Plant 63, 20–32. https://doi.org/10.32615/bp.2019.003.

Kuraishi, S., Tasaki, K., Sakurai, N., Sadatoku, K., 1991. Changes in levels of cytokinins in etiolated squash seedlings after illumination. Plant Cell Physiol. 32, 585–591. https://doi.org/10.1093/oxfordjournals.pcp.a078120.

Laemmli, U.K., 1970. Cleavage of structural proteins during the assembly of the head of bacteriophage T4. Nature 227, 680–685. https://doi.org/10.1038/227680a0.

Liu, D., Lin, Y., Wang, X., 2012a. Effects of lanthanum on growth, element uptake, and oxidative stress in rice seedlings. J. Plant Nutr. Soil Sci. 175, 907–911. https://doi.org/10.1002/jpln.201200016.

Liu, D., Wang, X., Lin, Y., Chen, Z., Xu, H., Wang, L., 2012b. The effects of cerium on the growth and some antioxidant metabolisms in rice seedlings. Environ. Sci. Pollut. Res. 19, 3282–3291. https://doi.org/10.1007/s11356-012-0844-x.

Liu, D., Wang, X., Zhang, X., Gao, Z., 2013. Effects of lanthanum on growth and accumulation in roots of rice seedlings. Plant Soil Environ. 59, 196–200. https://doi.org/10.17221/760/2012-PSE.

Liu, Z., Yu, Y., Kang, W., Chen, F., Yan, F., Ma, B., Ge, S., 2022. Self-assembled terbium-amino acid nanoparticles as a model for terbium biosafety and bone repair ability assessment. Compos. B Eng., 110186 https://doi.org/10.1016/j.compositesb.2022.110186.

Loktyushkin, A., Lovyagina, E., Semin, B., 2019. Interaction of terbium cations with the donor side of photosystem II in higher plants. Moscow Univ. Biol. Sci. Bull. 74, 81–85. https://doi.org/10.3103/S009639251902007X.

Ma, Y., Zhang, P., Zhang, Z., He, X., Li, Y., Zhang, J., Zheng, L., Chu, S., Yang, K., Zhao, Y., 2015. Origin of the different phytotoxicity and biotransformation of cerium and lanthanum oxide nanoparticles in cucumber. Nanotoxicology 9, 262–270. https://doi.org/10.3109/17435390.2014.921344.

Mittler, R., Zilinskas, B.A., 1993. Detection of ascorbate peroxidase-activity in native gels by inhibition of the ascorbate-dependent reduction of nitroblue tetrazolium. Anal. Biochem. 212, 540–546. https://doi.org/10.1006/abio.1993.1366.

Mubarik, M.S., Khan, S.H., Sajjad, M., Raza, A., Hafeez, M.B., Yasmeen, T., Rizwan, M., Ali, S., Arif, M.S., 2021. A manipulative interplay between positive and negative regulators of phytohormones: a way forward for improving drought tolerance in plants. Physiol. Plantarum 172, 1269–1290. https://doi.org/10.1111/ppl.13325.

Nakano, Y., Asada, K., 1981. Hydrogen peroxide is scavenged by ascorbate-specific peroxidase in spinach chloroplasts. Plant Cell Physiol. 22, 867–880. https://doi.org/10.1093/oxfordjournals.pcp.a076232.

Nyomora, A., Sah, R., Brown, P.H., Miller, R., 1997. Boron determination in biological materials by inductively coupled plasma atomic emission and mass spectrometry: effects of sample dissolution methods. Fresenius' J. Anal. Chem. 357, 1185–1191. https://doi.org/10.1007/s002160050328.

Oliveira, C., Gomes, B.C.R., Pelegrino, M.T., Seabrac, A.B., 2016. Nitric oxide-releasing chitosan nanoparticles alleviate the effects of salt stress in maize plants. Nitric Oxide 61, 10–19. https://doi.org/10.1016/j.niox.2016.09.010.

Palni, L.M.S., Summons, R.E., Letham, D.S., 1983. Mass spectrometric analysis of cytokinins in plant tissues: V. Identification of the cytokinin complex of *Datura innoxia* crown gall tissue. Plant Physiol. 72, 858–863. https://doi.org/10.1104/pp.72.3.858.

Paola, I.M., Paciolla, C., d'Aquino, L., Morgana, M., Tommasi, F., 2007. Effect of rare earth elements on growth and antioxidant metabolism in *Lemna minor* L. Caryologia 60, 125–128. https://doi.org/10.1080/00087114.2007.10589559.

Paradiso, A., Berardino, R., de Pinto, M.C., Sanita di Toppi, L., Storelli, M.M., Tommasi, F., De Gara, L., 2008. Increase in ascorbate-glutathione metabolism as local and precocious systemic responses induced by cadmium in durum wheat plants. Plant Cell Physiol. 49, 362–374. https://doi.org/10.1093/pcp/pcn013.

Qamaruddin, M., 1991. Appearance of the zeatin riboside type of cytokinin in *Pinus sylvestris* seeds after red light treatment. Scand. J. For. Res. 6, 41–46. https://doi.org/10.1080/02827589109382645.

Rachappanavar, V., Padiyal, A., Sharma, J.K., Gupta, S.K., 2022. Plant hormone-mediated stress regulation responses in fruit crops-a review. Sci. Hortic. 304, 111302 https://doi.org/10.1016/j.scienta.2022.111302.

Rajput, V.D., Singh, R.K., Verma, K.K., Sharma, L., Quiroz-Figueroa, F.R., Meena, M., Gour, V.S., Minkina, T., Sushkova, S., Mandzhieva, S., 2021. Recent developments in enzymatic antioxidant defence mechanism in plants with special reference to abiotic stress. Biology 10, 267. https://doi.org/10.3390/biology10040267.

Ramos, S.J., Dinali, G.S., Oliveira, C., Martins, G.C., Moreira, C.G., Siqueira, J.O., Guilherme, L.R., 2016. Rare earth elements in the soil environment. Curr. Pollut. Rep. 2, 28–50. https://doi.org/10.1007/s40726-016-0026-4.

Rao, K.M., Sresty, T., 2000. Antioxidative parameters in the seedlings of pigeonpea (*Cajanus cajan* (L.) Millspaugh) in response to Zn and Ni stresses. Plant Sci. 157, 113–128. https://doi.org/10.1016/S0168-9452(00)00273-9.

Rhaman, M.S., Imran, S., Rauf, F., Khatun, M., Baskin, C.C., Murata, Y., Hasanuzzaman, M., 2020. Seed priming with phytohormones: an effective approach for the mitigation of abiotic stress. Plants 10, 37. https://doi.org/10.3390/plants10010037.

Ricci, G., Bello, M.L., Caccuri, A.M., Galiazzo, F., Federici, G., 1984. Detection of glutathione transferase activity on polyacrylamide gels. Anal. Biochem. 143, 226–230. https://doi.org/10.1016/0003-2697(84)90657-2.

Rodziewicz, P., Swarcewicz, B., Chmielewska, K., Wojakowska, A., Stobiecki, M., 2014. Influence of abiotic stresses on plant proteome and metabolome changes. Acta Physiol. Plant. 36, 1–19. https://doi.org/10.1007/s11738-013-1402-y.

Sagi, M., Fluhr, R., 2001. Superoxide production by plant homologues of the gp91phox NADPH oxidase. Modulation of activity by calcium and by tobacco mosaic virus infection. Plant Physiol. 126, 1281–1290. https://doi.org/10.1104/pp.126.3.1281.

Salem, S.S., Fouda, A., 2021. Green synthesis of metallic nanoparticles and their prospective biotechnological applications: an overview. Biol. Trace Elem. Res. 199, 344–370. https://doi.org/10.1007/s12011-020-02138-3.

Salvi, P., Manna, M., Kaur, H., Thakur, T., Gandass, N., Bhatt, D., Muthamilarasan, M., 2021. Phytohormone signaling and crosstalk in regulating drought stress response in plants. Plant Cell Rep. 40, 1305–1329. https://doi.org/10.1007/s00299-021-02683-8.

Sameena, P., Puthur, J.T., 2021. Differential modulation of photosynthesis and defense strategies towards copper toxicity in primary and cotyledonary leaves of *Ricinus communis* L. J. Photochem. Photobiol., A 8, 100059. https://doi.org/10.1016/j.jpap.2021.100059.

Seevers, P., Daly, J., Catedral, F., 1971. The role of peroxidase isozymes in resistance to wheat stem rust disease. Plant Physiol. 48, 353–360. https://doi.org/10.1104/pp.48.3.353.

Shamsipur, M., Pashabadi, A., 2018. Latest advances in PSII features and mechanism of water oxidation. Coord. Chem. Rev. 374, 153–172. https://doi.org/10.1016/j.ccr.2018.07.006.

Shan, C., Wang, B., Sun, H., Gao, S., Li, H., 2020. H_2S induces NO in the regulation of AsA-GSH cycle in wheat seedlings by water stress. Protoplasma 257, 1487–1493. https://doi.org/10.1007/s00709-020-01510-3.

Shi, H., Ye, T., Chan, Z., 2013. Exogenous application of hydrogen sulfide donor sodium hydrosulfide enhanced multiple abiotic stress tolerance in bermudagrass (*Cynodon dactylon* (L). Pers.). Plant Physiol. Biochem. 71, 226–234. https://doi.org/10.1016/j.plaphy.2013.07.021.

Soliman, S., Abu-Zied, B., 2009. Thermal genesis, characterization, and electrical conductivity measurements of terbium oxide catalyst obtained from terbium acetate. Thermochim. Acta 491, 84–91. https://doi.org/10.1016/j.tca.2009.03.006.

Song, W., Hong, F., Wan, Z., Zhou, Y., 2002. Effects of lanthanum and europium on rooting of plantlet *Etiobotrya japonica* Lindl. in vitro. J. Rare Earths 20, 658–662.

Syrvatka, V., Rabets, A., Gromyko, O., Luzhetskyy, A., Fedorenko, V., 2022. Scandium–microorganism interactions in new biotechnologies. Trends Biotechnol. 40 (9), 1088–1101. https://doi.org/10.1016/j.tibtech.2022.02.006.

Wang, L., Li, J., Zhou, Q., Yang, G., Ding, X.L., Li, X., Cai, C.X., Zhang, Z., Wei, H.Y., Lu, T.H., 2014. Rare earth elements activate endocytosis in plant cells. Proc. Natl. Acad. Sci. U.S.A. 111, 12936–12941. https://doi.org/10.1073/pnas.1413376111.

Wang, L., Zhou, Q., Huang, X., 2009. Photosynthetic responses to heavy metal terbium stress in horseradish leaves. Chemosphere 77, 1019–1025. https://doi.org/10.1016/j.chemosphere.2009.07.065.

Woodbury, W., Spencer, A., Stahmann, M., 1971. An improved procedure using ferricyanide for detecting catalase isozymes. Anal. Biochem. 44, 301–305. https://doi.org/10.1016/0003-2697(71)90375-7.

Xiao, R., Huang, W., Xiao, X., Liu, Y., Guo, D., 2019. Novel salicyloylhydrazone derivatives and corresponding terbium (III) complexes: synthesis and properties research. Luminescence 34, 90–97. https://doi.org/10.1002/bio.3583.

Xiaoqing, L., Hao, H., Chao, L., Min, Z., Fashui, H., 2009. Physico-chemical property of rare earths-effects on the energy regulation of photosystem II in *Arabidopsis thaliana*. Biol. Trace Elem. Res. 130, 141–151. https://doi.org/10.1007/s12011-009-8321-1.

Xu, X., Wang, Z., 2007. Phosphorus uptake and translocation in field-grown maize after application of rare earth-containing fertilizer. J. Plant Nutr. 30 (4), 557–568. https://doi.org/10.1080/01904160701209287.

Yang, L., Wang, Z., Xu, L., 2006. Simultaneous determination of phenols (bibenzyl, phenanthrene, and fluorenone) in *Dendrobium* species by high-performance liquid chromatography with diode array detection. J. Chromatogr. A 1104, 230–237. https://doi.org/10.1016/j.chroma.2005.12.012.

Yao, R., Li, Y., Chen, Y., Xu, B., Chen, C., Zhang, C., 2021. Rare-earth elements can structurally and energetically replace the calcium in a synthetic Mn_4CaO_4-cluster mimicking the oxygen-evolving center in photosynthesis. J. Am. Chem. Soc. 143, 17360–17365. https://doi.org/10.1021/jacs.1c09085.

Zhang, C., Li, Q., Zhang, M., Zhang, N., Li, M., 2013. Effects of rare earth elements on growth and metabolism of medicinal plants. Acta Pharm. Sin. B. 3, 20–24. https://doi.org/10.1016/j.apsb.2012.12.005.

Zicari, M.A., d'Aquino, L., Paradiso, A., Mastrolitti, S., Tommasi, F., 2018. Effect of cerium on growth and antioxidant metabolism of Lemna minor L. Ecotoxicol. Environ. Saf. 163, 536–543. https://doi.org/10.1016/j.ecoenv.2018.07.113.

Zulfiqar, F., Ashraf, M., 2022. Antioxidants as modulators of arsenic-induced oxidative stress tolerance in plants: an overview. J. Hazard Mater. 127891 https://doi.org/10.1016/j.jhazmat.2021.127891.